# Lithium Peroxide Surfaces Are Metallic, While Lithium Oxide Surfaces Are Not

Maxwell D. Radin,[†] Jill F. Rodriguez,[‡] Feng Tian,[‡] and Donald J. Siegel*[,‡,§,‖]

[†]Department of Physics, [‡]Mechanical Engineering Department, [§]Applied Physics Program, and [‖]Michigan Energy Institute, University of Michigan, Ann Arbor, Michigan 48109-2125, United States
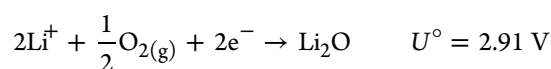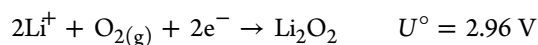
S Supporting Information

ABSTRACT: The thermodynamic stability and electronic structure of 40 surfaces of lithium peroxide (Li_2O_2) and lithium oxide (Li_2O) were characterized using first-principles calculations. As these compounds constitute potential discharge products in Li−oxygen batteries, their surface properties are expected to play a key role in understanding electrochemical behavior in these systems. Stable surfaces were identified by comparing 23 distinct Li_2O_2 surfaces and 17 unique Li_2O surfaces; crystallite areal fractions were determined through application of the Wulff construction. Accounting for the oxygen overbinding error in density functional theory results in the identification of several new Li_2O_2 oxygen-rich $\{0001\}$ and $\{1\bar{1}00\}$ terminations that are more stable than those previously reported. Although oxygen-rich facets predominate in Li_2O_2, in Li_2O stoichiometric surfaces are preferred, consistent with prior studies. Surprisingly, surface-state analyses reveal that the stable surfaces of Li_2O_2 are half-metallic, despite the fact that Li_2O_2 is a bulk insulator. Surface oxygens in these facets are ferromagnetic with magnetic moments ranging from 0.2 to 0.5 μ_B. In contrast, the stable surfaces of Li_2O are insulating and nonmagnetic. The distinct surface properties of these compounds may explain observations of electrochemical reversibility for systems in which Li_2O_2 is the discharge product and the irreversibility of systems that discharge to Li_2O. Moreover, the presence of conductive surface pathways in Li_2O_2 could offset capacity limitations expected to arise from limited electron transport through the bulk.

Li₂O (111)   Li₂O₂ (0001)
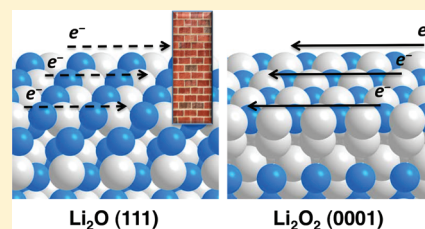
1. INTRODUCTION

Many technologies stand to benefit from high-density energy storage. Prominent examples include battery-powered electric vehicles and the adoption of intermittent, renewable power sources (i.e., wind and solar) on the electrical grid. The state-of-the-art rechargeable battery, Li-ion, is costly and suffers from relatively low specific energy densities of ~150 (W h)/kg (system level)[1] that are inadequate for applications requiring large energy densities.[2] The Li−oxygen battery is an alternative chemistry that uses atmospheric oxygen as a reactant and may offer a significant increase in specific energy density.[1,3,4] Depending on the composition of the discharge product, practical estimates of the specific energy range from 2500 to 3700 (W h)/kg (cathode).[5]

In the absence of solvent degradation[6−10] the discharge of Li−O₂ batteries can potentially occur via two reactions, wherein the product phase is an insoluble solid peroxide (Li_2O_2) or oxide (Li_2O):[11]

$$2Li^+ + O_{2(g)} + 2e^- \rightarrow Li_2O_2 \qquad U^\circ = 2.96 \text{ V}$$

$$2Li^+ + \frac{1}{2}O_{2(g)} + 2e^- \rightarrow Li_2O \qquad U^\circ = 2.91 \text{ V}$$

Abraham et al. were the first to demonstrate a prototype *rechargeable* Li−air battery consisting of a lithium metal anode and an air-breathing carbon cathode separated by a Li⁺ conductive polymer electrolyte membrane.[12] Raman spectra indicated that the primary discharge product was Li_2O_2,[12]

which has been confirmed by subsequent experiments.[6,13−16] However, the formation of Li_2O has also been suggested in other studies,[15,17−20] albeit with some degree of uncertainty due to the possibility of decomposition of carbonate-based solvents. Nevertheless, recent studies employing carbonate-free systems (e.g., refs 15 and 20) note the existence of Li_2O peaks in X-ray diffraction spectra for cells discharged to low potentials. Subsequent charging experiments have confirmed that Li_2O_2 decomposes to Li and O_2 during recharge.[5,16] Li_2O, on the other hand, is believed to be electrochemically irreversible.[21,57,58] Given the similar thermodynamic and electronic properties of these compounds—both Li_2O_2 and Li_2O are bulk insulators and have similar formation energies (see below)—their differing behavior with regard to reversibility is somewhat surprising. While the mechanisms underlying these differences are of relevance for the performance of Li−oxygen cells, they are not well understood.

Despite growing interest in Li−oxygen batteries,[3−10,12−29,31,33] Li−oxygen technology remains in its infancy, and several performance gaps must be overcome to achieve a viable rechargeable system. These include (i) low efficiencies caused by high overpotentials during charging,[4] (ii) low rates of charge/discharge, and (iii) poor capacity retention. Although use of cathode catalysts[5,13,26−29] has been shown to moderately improve rate capability and reversibility, efficiency

remains poor overall (<∼70%); thus, further improvements are highly desirable. Moreover, the key mechanisms that limit the performance of Li−oxygen systems are only now beginning to emerge. For example, the structure, composition, and electronic proprieties of the primary discharge phases Li_2O_2 and Li_2O have not been systematically characterized and correlated with battery performance. Lacking this information, the optimization of Li−oxygen systems appears to be progressing in an Edisonian fashion.

One factor that may influence the performance of Li−oxygen cells is the surface properties of Li−O product phases. Depending on discharge rate, the morphologies of Li_2O_2 deposits formed during discharge range from discrete particles with nanometer-scale diameters to thin films.[14] The low-energy facets of these phases are expected to be the locus of important reaction and mass transport processes, which would in turn impact the rate and overpotential associated with discharge. (In principle, surface phenomena may also play a role during charging; however, the mechanisms associated with the decomposition of Li_2O_2/Li_2O are at present unclear.) As the relative stability of a compound's surfaces determines the equilibrium shape of its crystallites,[30] those surfaces having low energies will comprise larger fractions of the crystallite's surface area and as a consequence have outsized effects on surface reactions.

Another factor that can impact the performance of Li−oxygen batteries is electron transport through the Li_2O_2/Li_2O discharge phases. In bulk form these compounds are insulators, with band gaps ranging from 2 eV (based on our and others' DFT calculations) to 5 eV (GW calculations[23,31]) in Li_2O_2 and band gaps of approximately 8 eV in Li_2O.[32] Using these insulating properties as input, Albertus et al.[31] recently developed a macrohomogeneous model of the Li−oxygen battery. Their model revealed that passivation by the resistive discharge products was a major obstacle to achieving high capacities. Although an important result, the model assumed an idealized monolithic discharge phase and therefore did not account for the microstructural features (e.g., small Li_2O_2 particles with exposed surfaces) observed in realistic discharge experiments. Calculations by Chen et al. found that electron transport through interfaces comprised of Li_2O_2 and Au or Pt depends sensitively upon the orientation and lattice matching of the interface.[33] Furthermore, X-ray diffraction and X-ray absorption near-edge spectroscopy (XANES) data suggest that the discharge phases are polycrystalline and possibly sub-stoichiometric.[14] Taken together, these observations suggest that electron transport in Li_2O and Li_2O_2 may not be well-approximated by transport in pristine bulk phases.[33] For example, Hummelshøj et al. have shown that Li_2O_2 exhibits metallic behavior[23] in the limit of very high concentrations (∼6 atom %) of Li vacancies. Consequently, if surfaces and other planar defects such as grain boundaries exhibit lithium-poor stoichiometries, then localized metallic behavior and facile electron transport within these regions could result.

Given the predominance of particle and (potentially) polycrystalline morphologies in Li−oxygen discharge phases, a sound understanding of the thermodynamics, composition, and electronic structure of the surfaces of these phases would appear to be a prerequisite for revealing performance-limiting phenomena in Li−oxygen batteries. However, despite their importance, relatively little work has been devoted to these issues. The most comprehensive study of Li−O surfaces to date is that of Seriani,[24] who examined a small set of candidate

surfaces consisting of nine Li_2O surfaces (three terminations were examined from each of the {111}, {110}, and {100} normals) and seven Li_2O_2 surfaces (three of which were basal surfaces and four of which were {11$\bar{2}$0} surfaces).[24] [Although the authors of ref 24 mention calculations on Li_2O_2 {1$\bar{1}$00} surfaces, the images shown in their Figures b−e are of {11$\bar{2}$0} surfaces. This, combined with trends in their reported surface energies, led us to conclude that calculations described as {1$\bar{1}$00} surface calculations were actually performed on {11$\bar{2}$0} surfaces.] In addition to exploring a wider range of candidate surfaces—including the important {1$\bar{1}$00} prismatic surfaces of Li_2O_2—in this study we systematically account for finite-temperature thermodynamic contributions and for the well-known O_2 overbinding error present in density functional theory (DFT). Omission of the overbinding correction in ref 24 resulted in the prediction that Li_2O was the stable bulk phase under ambient conditions, in disagreement with experiments.[11,34] Given its important effect on bulk stabilities, it is clear that the O_2 overbinding error will also impact the relative stabilities of surfaces. Although not a comprehensive study, Hummelshøj and co-workers have reported calculations on a prismatic surface of Li_2O_2, which they identified as the most stable among several low-index surfaces.[23]

Toward the goal of linking battery performance to materials properties, in the present study we use DFT calculations to systematically characterize the stability and electronic structure of 40 distinct surfaces of Li_2O_2 and Li_2O. Stable surfaces were identified at realistic temperatures and pressures by comparing the free energies of 23 distinct Li_2O_2 surfaces and 17 unique Li_2O surfaces. Equilibrium crystallite shapes and the relative areal fractions of low-energy facets were predicted using the Wulff construction.[30] For Li_2O_2, we identify several new oxygen-rich {0001} and {1$\bar{1}$00} facets which are more stable than those previously reported in the literature. For Li_2O a single stoichiometric {111} surface is found to be most stable, consistent with a prior study.[24] Despite the fact that Li_2O_2 is an insulator, surface state analyses surprisingly reveal that its stable surfaces are *metallic and magnetic*, and we derive an estimate for the electrical conductivity in the metallic surface region. In contrast, the stable surfaces of Li_2O are *insulating and nonmagnetic*. The distinct surface properties exhibited by these compounds will strongly impact their respective electrochemical reactivities and may explain the origin of differing rechargeability of Li_2O_2 and Li_2O in Li−oxygen batteries.

2. COMPUTATIONAL METHODS

First-principles calculations were performed using the Perdew−Burke−Ernzerhof (PBE) generalized gradient approximation (GGA)[35] to DFT, as implemented in the Vienna Ab-initio Simulation Package (VASP).[36−39] Projector-augmented wave (PAW) potentials[40,41] were employed with valence states of 2s for Li and 2s2p for O, and spin-polarized calculations were used for all surface and molecular geometries. A cutoff energy of 400 eV was used for the plane wave basis, in conjunction with the Monkhorst−Pack scheme[42] for k-point sampling. A Gaussian smearing of 0.2 eV for the Fermi−Dirac distribution function was used for bulk and surface calculations; a much smaller width of 0.01 eV was used in the case of molecules. For geometric optimizations, all ions were relaxed to a force tolerance of 0.02 eV/Å or less. For bulk calculations, the unit cells consisted of 8 atoms for Li_2O_2, 12 atoms for Li_2O, and 2 atoms for body-centered cubic (bcc) Li. These cells were sampled with k-point meshes of 4 × 4 × 2, 6 × 6 × 6, and 10 × 10 × 10, respectively.

To identify low-energy surfaces, we performed a search over 23 distinct surfaces of Li_2O_2 and 17 surfaces of Li_2O. In the case of Li_2O_2 we examined 6 basal plane {0001} surfaces, 10 {1$\bar{1}$00} surfaces, and 7

$\{11\bar{2}0\}$ surfaces by altering the surface termination/slab stoichiometry through selective removal of oxygen or lithium atoms. A similar strategy was used to construct candidate Li_2O surfaces, resulting in six $\{100\}$ surfaces, eight $\{110\}$ sufaces, and three $\{111\}$ surfaces. In some cases the cell was doubled in one (2×1) direction of the surface plane to accommodate these stoichiometries. Each surface unit cell employed a slab geometry with a ~10 Å vacuum region in the direction normal to the surfaces. k-point meshes for the Li_2O_2 $\{0001\}$ surfaces with (1×1) and (2×1) supercells were respectively $6 \times 6 \times 1$ and $4 \times 6 \times 1$. The k-point mesh for Li_2O_2 $\{11\bar{2}0\}$ surfaces and Li_2O_2 $\{1\bar{1}00\}$ surfaces was $8 \times 6 \times 1$. The k-point mesh was set at $6 \times 6 \times 1$ for all Li_2O surfaces.

Vibrational contributions to the free energies of all surface and bulk phases were evaluated within the harmonic approximation,[43] with normal-mode vibrational frequencies calculated using the direct method, as previously described.[44] The vibrational frequencies of Li_2O_2 $\{0001\}$ and all Li_2O surfaces were calculated using enlarged 2×2 supercells, while those for Li_2O_2 $\{11\bar{2}0\}$ and $\{1\bar{1}00\}$ were calculated in 2×1 geometries. For the free energy of gas-phase O_2 we include enthalpic contributions of $^7/_2 k_B T$ from translational, rotational, and pV degrees of freedom and entropic contributions from tabulated experimental data.[11] Pressure contributions to the free energy of O_2 are given by $k_B T \ln(P/P_0)$.

To correct for the well-known overbinding of the O_2 molecule within DFT,[45,46] we employ the experimental binding energy of O_2, $\Delta E^{exptl} = 5.12$ eV:[11]

$$H(T = 0 \text{ K}, O_2) = 2H(T = 0 \text{ K}, O) - \Delta E^{exptl}$$

where $H(T = 0 \text{ K}, X)$ is the calculated ground-state energy of an oxygen $(X = O)$ atom or oxygen molecule $(X = O_2)$. Following this approach, we obtain a corrected value for the static energy of O_2 that is 0.86 eV higher than the value obtained from direct calculations involving an isolated O_2 molecule. As demonstrated in Table 1, this

Table 1. Enthalpies and Free Energies of Formation (eV) at 300 K for Li_2O_2 and Li_2O from Calculations and Experiments

		this work	other calculations	experiments[d]
Li_2O_2	ΔH_f^O	−6.59	−5.57[a]	−6.57
	ΔG_f^O	−5.99	−4.94,[a] −5.41,[b] −4.98[c]	−5.92
Li_2O	ΔH_f^O	−6.03		−6.22
	ΔG_f^O	−5.62	−5.29[b]	−5.83

[a]Reference 23. [b]Reference 22. [c]Reference 24. [d]Reference 11.

choice of correction leads to calculated formation energies of Li_2O_2 and Li_2O in excellent agreement with experimental data. The size of our proposed correction is larger than that obtained from approaches employing a thermodynamic cycle based on the experimental formation energy of molecular H_2O,[22,23] from which we find a correction of 0.39 eV. However, in our experience this approach results in significant underestimates of the formation energies (up to 1 eV/fu (formula unit)) of many solid oxides (see ref 46 and the summary of other DFT calculations in Table 1). Wang et al. have proposed an alternative approach based on the formation energies of several non-transition-metal solid oxide phases.[46] Since that approach avoids the use of molecular energies, in principle it should yield more reliable results. However, the calculated correction (1.36 eV) was found to be significantly larger than the experimental value, presumably due to errors associated with charge transfer to oxygen p orbitals. Our tests reveal that this correction also yields less accurate predictions of formation energies.

3. CALCULATION OF SURFACE ENERGIES

Surface free energies as a function of temperature and pressure were determined using the methodology described by Reuter and Scheffler.[47] In general, the surface free energy $\gamma(T,P)$ of a

Li_2O_2 or Li_2O surface at a temperature T and pressure P is given by

$$\gamma(T, P) = \frac{1}{2A}[G^{slab}(T, P, N_{Li}, N_O) - N_{Li}\mu_{Li}(T, P) - N_O\mu_O(T, P)] \quad (1)$$

where G^{slab} is the free energy of the surface supercell, A is the area, N_{Li} and N_O are the numbers of Li and O atoms present in the slab, and $\mu_{Li}(T,P)$ and $\mu_O(T,P)$ are the chemical potentials of Li and O in bulk Li_2O_2 or Li_2O. For Li_2O_2 this expression can be written in terms of the free energy per formula unit of bulk Li_2O_2 ($g_{Li_2O_2}^{bulk}$) and the chemical potential of oxygen:

$$\gamma_{Li_2O_2}(T, P) = \frac{1}{2A}\bigg[G^{slab}(T, P, N_{Li}, N_O) - \frac{1}{2}N_{Li}g_{Li_2O_2}^{bulk}(T, P) + (N_{Li} - N_O)\mu_O(T, P)\bigg] \quad (2)$$

A similar equation can be derived for Li_2O:

$$\gamma_{Li_2O}(T, P) = \frac{1}{2A}\bigg[G^{slab}(T, P, N_{Li}, N_O) - \frac{1}{2}N_{Li}g_{Li_2O}^{bulk}(T, P) + \left(\frac{1}{2}N_{Li} - N_O\right)\mu_O(T, P)\bigg] \quad (3)$$

Assuming thermodynamic equilibrium, the chemical potential of oxygen μ_O in Li_2O_2 is determined by the pressure and temperature of gas-phase O_2. Since experimentally μ_O cannot be varied without bounds, it is conventional to limit its possible values; for Li_2O_2, we employ the following limits:

$$\mu_O^{O_2}(300 \text{ K}, 1000 \text{ atm}) + \frac{1}{2}\Delta G_f^{Li_2O_2}(300 \text{ K}, 1 \text{ atm}) < \mu_O(T, P) < \mu_O^{O_2}(300 \text{ K}, 1000 \text{ atm}) \quad (4)$$

Here $\mu_O^{O_2}$ is the chemical potential per oxygen atom in gas-phase O_2 and ΔG_f is the (negative) formation energy of Li_2O_2 (with respect to Li metal and gas-phase O_2). The upper limit on μ_O corresponds to an oxygen-rich environment (i.e., high O_2 pressure), while the lower limit corresponds to an oxygen-poor environment (i.e., pressures low enough that Li_2O_2 may decompose to bcc lithium and gas-phase oxygen). For Li_2O, we use analogous limits:

$$\mu_O^{O_2}(300 \text{ K}, 1000 \text{ atm}) + \Delta G_f^{Li_2O}(300 \text{ K}, 1 \text{ atm}) < \mu_O(T, P) < \mu_O^{O_2}(300 \text{ K}, 1000 \text{ atm}) \quad (5)$$

These bounds are formal estimates of the physical limits and serve as reference points on the μ_O axis. We assume a fixed temperature of 300 K; thus, variations in μ_O correspond to changes in the pressure of gas-phase O_2. We note that under these conditions the oxygen-poor limit corresponds to extremely low pressures (~10^{-100} atm); we therefore focus

our attention on a more realistic range of 10^{-15}–10^3 atm. In our analysis we compare several candidate surfaces; the surface having the lowest free energy at a given μ_O corresponds to the most stable termination.

4. RESULTS AND DISCUSSION

4.1. Bulk Phases. The hexagonal crystal structure of Li_2O_2 with $P6_3/mmc$ symmetry from Föppl[48] and Cota et al.[49] (Figure
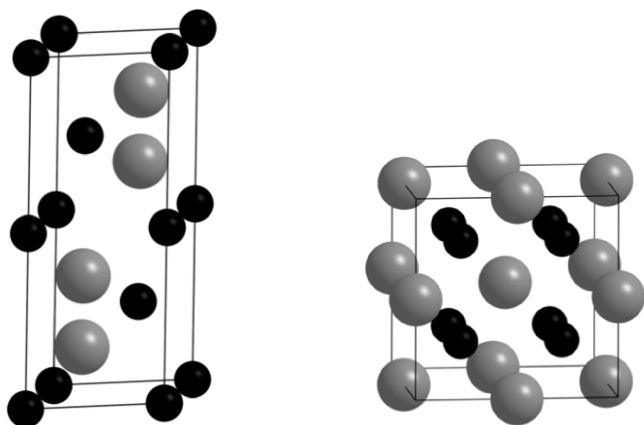
Figure 1. Unit cell for (left) bulk Li_2O_2 and (right) bulk Li_2O. Gray and black spheres represent O and Li atoms, respectively.

1) was adopted to model bulk Li_2O_2. In this structure oxygen appears as a complex O_2 anion. Lattice constants were optimized and found to be $a = 3.16$ Å and $c = 7.69$ Å, in good agreement with the reported values of 3.14 and 7.65 Å from experiments[48] and 3.18 and 7.73 Å from DFT calculations.[49] The O–O bond length in the O_2 anionic dimer was calculated to be 1.55 Å, which is close to the value of 1.57 Å reported by Seriani[24] and slightly longer than the bond length in gas-phase O_2 (1.21 Å).[50] The lattice constants for Li_2O, which crystallizes in the cubic antifluorite structure (Figure 1), and bcc Li were calculated to be 4.63 and 3.44 Å, respectively. These values agree well with the experimental values of 4.62 Å[51] and 3.48 Å.[52]

Table 1 summarizes our calculated enthalpies and free energies of formation for Li_2O_2 and Li_2O at $T = 300$ K. In contrast to some prior calculations, our predicted values correctly reflect the relative stabilities of these phases and exhibit relatively small deviations (<4%) from the experimental measurements. This improvement can be attributed to the use of the experimental O_2 overbinding correction, as previously described. (Since the experimental formation energies of Li_2O and Li_2O_2 differ by less than 0.1 eV/fu, these compounds are practically degenerate in DFT given errors typical of these calculations.)

4.2. Surface Stability. *4.2.1. Li_2O_2 Surfaces.* The calculated free energies of 23 low-index Li_2O_2 surfaces with Miller indices of $\{0001\}$, $\{1\bar{1}00\}$, and $\{11\bar{2}0\}$ are plotted in Figure 2 as a function of oxygen chemical potential at 300 K. Likewise, Table 2 lists the surface energies of selected low-energy Li_2O_2 surfaces at 300 K and 1 atm. (The selection of the chemical potential at near-ambient conditions is based on the assumption of equilibrium among oxygen in Li_2O_2, oxygen dissolved in the electrolyte, and gas-phase O_2 at 1 atm.) Structures corresponding to the surfaces in Table 2 are shown in Figure 3. For a given Miller index, surfaces of different

stoichiometries were generated by cleavage at different depths followed by removal of selected lithium or oxygen atoms. (Structural models for all of the surfaces studied are included in the Supporting Information.) We adopt a naming convention wherein surface slabs that maintain the Li_2O_2 or Li_2O stoichiometry are abbreviated as "stoichi" and slabs that are rich in oxygen or lithium are respectively denoted "O-rich" or "Li-rich". Structures denoted "half-oxy" were constructed by removing half the oxygen atoms from the surfaces of a stoichiometric slab and are thus slightly Li-rich. (We emphasize that in the present study the term "stoichiometry" refers to the stoichiometry of the *entire surface slab*, and not necessarily to the local stoichiometry of the surface proper. Thus, it is possible to have oxygen-rich slabs whose immediate surface layers are stoichiometric.) The different stoichiometries are reflected in the different slopes for the respective surface free energies. Stoichiometric surface slabs have a slope of zero and are independent of the oxygen chemical potential, whereas O-rich (Li-rich) surfaces have negative (positive) slopes. The upper limit for the oxygen chemical potential, which corresponds to the O-rich case, is defined as zero for convenience; consequently, the lower limit (O-poor case) is given by $^1/_2\Delta G_f^{Li_2O_2}$(300 K, 1 atm) for Li_2O_2 and $\Delta G_f^{Li_2O}$(300 K, 1 atm) for Li_2O, as in eqs 4 and 5.

Turning first to the (basal) $\{0001\}$ surface of Li_2O_2, we find that the O-rich-1 stoichiometry is the most stable at 300 K and 1 atm (Figure 2, top left panel) and the most stable Li_2O_2 surface overall. The structure of this surface consists of intact O_2 dimers aligned parallel to the surface normal, with alternating layers of O^- and Li^+ ions, consistent with the structure of a polar surface. (We find that terminations that cleave the O–O bond exhibit much higher surface formation energies.) Electrostatic models of surfaces typically favor nonpolar configurations; thus, the appearance of a stable polar configuration is somewhat surprising.[53,54] However, it is possible to stabilize polar surfaces through charge compensation achieved by filling of conduction band surface states or depletion of valence band surface states.[52,53] In the subsequent section we demonstrate that the latter mechanism is responsible for the stability of O-rich surfaces in Li_2O_2. Under these conditions of temperature and pressure, the surface energy of the O-rich-1 termination is 26 meV/Å^2 lower than that of the stoichi-2 surface, which is the next most stable structure. This result differs from the result of ref 24, who found that the stoichiometric slab was the most stable. This discrepancy primarily arises from treatment of the oxygen overbinding correction, which was omitted in ref 24 and which tends to favor O-rich stoichiometries. [The energy for an oxygen molecule, $E_0(O_2)$, used in ref 24 is −9.790 eV and is based on the Perdew–Wang 1991 (PW91) GGA. Our $E_0(O_2)$ employs the PBE GGA and is given by −9.859 eV plus an overbinding correction of 0.857 eV for a total of −9.002 eV. For a typical surface with an area of 10 Å^2, this 0.788 eV difference in $E_0(O_2)$ will result in a difference in surface energy of around 20 meV/Å^2. We also note that our calculated energies for the stoichiometric surfaces, which are independent of the oxygen chemical potential, closely follow the trends reported in ref 24 but are on average slightly smaller by ∼5–9 meV/Å^2. This can be attributed to differences in computational methodology such as functionals, phonon contributions, pseudopotentials, and structure optimization.]

For the prismatic $\{1\bar{1}00\}$ surfaces of Li_2O_2 a set of three oxygen-rich terminations (O-rich-1, -2, and -3) are found to be
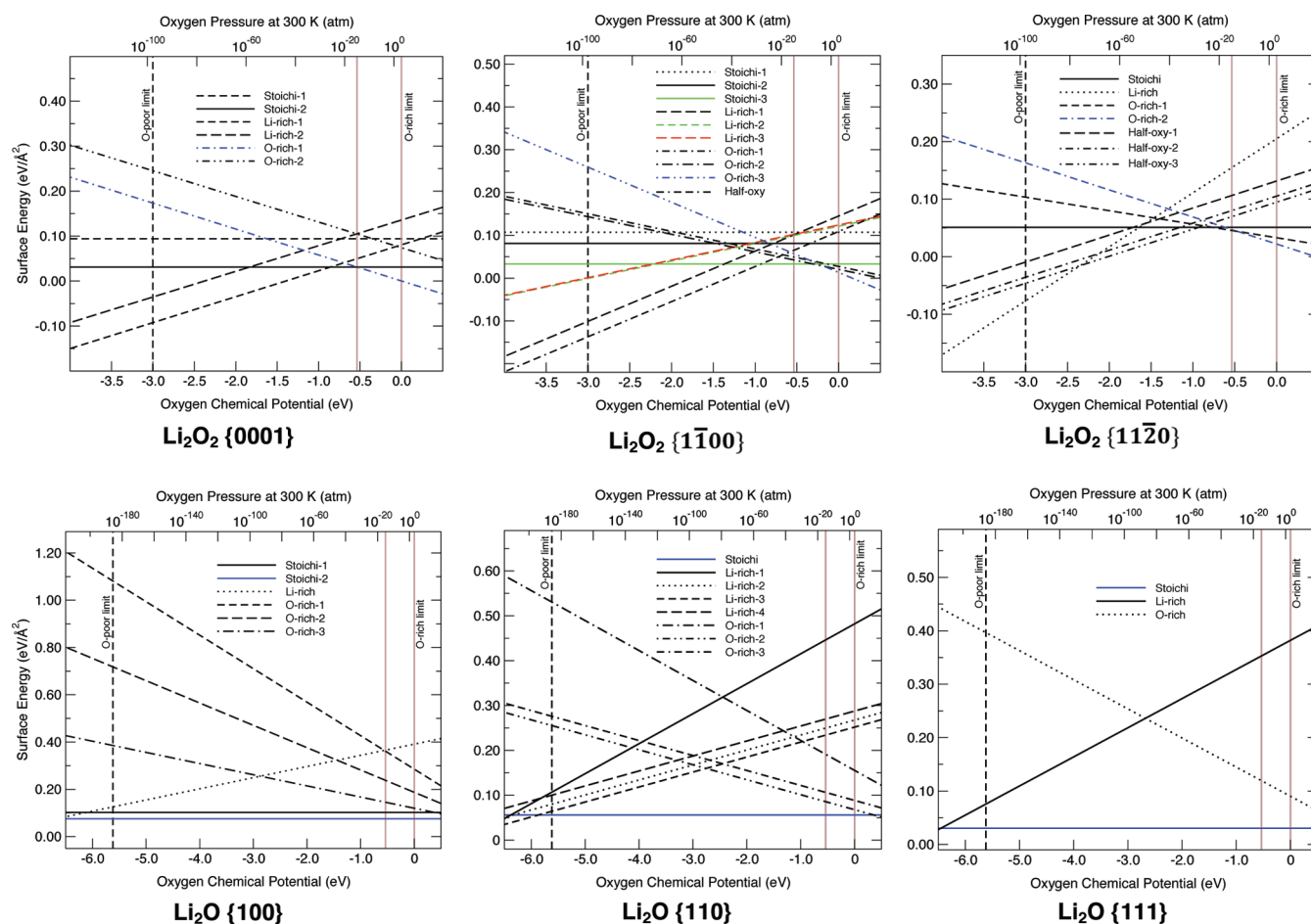
Figure 2. Free energies of candidate Li_2O_2 (top row) and Li_2O (bottom row) surfaces as a function of the oxygen chemical potential (lower axis) and O_2 partial pressure (top axis) at 300 K. Gray vertical lines delineate the experimentally accessible pressure range of 10^{-15}–10^3 atm. In each case the surface having the lowest surface energy at 1 atm is plotted in blue. The names "O-rich", "Li-rich", and "stoichi" denote oxygen-rich, lithium-rich, and stoichiometric slabs, respectively.

Table 2. Free Energies of Selected Li_2O_2 and Li_2O Surfaces at 300 K and $P(O_2) = 1$ atm[a]

|	surface index	surface name	surface free energy γ (meV/Å^2)	surface free energy γ (meV/atom)
Li_2O_2	{0001}	stoichi-2	32	185
		O-rich-1	6	26
	{1$\bar{1}$00}	stoichi-3	34	331–497
		O-rich-1	31	103–275
		O-rich-2	25	100–150
		O-rich-3	21	73–85
	{11$\bar{2}$0}	stoichi	52	275
		O-rich-1	36	217
		O-rich-2	26	80–187
Li_2O	{100}	stoichi	75	399–798
	{110}	stoichi	56	279
	{111}	stoichi	30	140–280

[a]The corresponding surface structures are shown in Figures 3 and 5. The free energy per surface atom is determined by dividing the formation energy per unit cell by the number of surface sites. In cases where the number of surface sites is ambiguous, a range of values is provided.

the most energetically favorable surfaces under ambient conditions (Figure 2, top middle panel). The most stable termination overall is the polar O-rich-3 surface, shown in

Figure 3. In comparison, the most stable {1$\bar{1}$00} surface predicted by Hummelshøj et al.[23] is the stoichi-3 surface, which they also reported as possessing the lowest surface energy among other low-index Li_2O_2 surfaces. As described for the basal surfaces, this difference arises mainly from the choice of oxygen overbinding correction. To the best of our knowledge, the authors of ref 24 did not examine {1$\bar{1}$00} surfaces.

Finally, for the {11$\bar{2}$0} surfaces of Li_2O_2, the most stable surface is the O-rich-2 surface with a free energy of 26 meV/Å^2. Seriani also identified this surface as a stable termination.[24] Given that the free energy of this surface is larger than the energies of the {0001} O-rich-1 surface (6 meV/Å^2) and {1$\bar{1}$00} O-rich-3 surface (21 meV/Å^2), it is expected to contribute less to the areal fraction of Li_2O_2 crystallites compared to the lower energy facets, as demonstrated below.

The calculated surface energies were used in conjunction with the Wulff construction[30] to predict the equilibrium shape of Li_2O_2 crystallites. As shown in Figure 4, at 300 K and 1 atm, Li_2O_2 adopts a low aspect ratio hexagonal prism morphology, with nearly two-thirds of its surface area consisting of basal O-rich-1 surfaces and the balance being prismatic {1$\bar{1}$00} O-rich-3 surfaces. Due to their higher surface energies in comparison to that of the prismatic surface, {11$\bar{2}$0} surface facets do not contribute to the crystallite area. The predominance of the oxygen-rich basal surface is consistent with it being the lowest
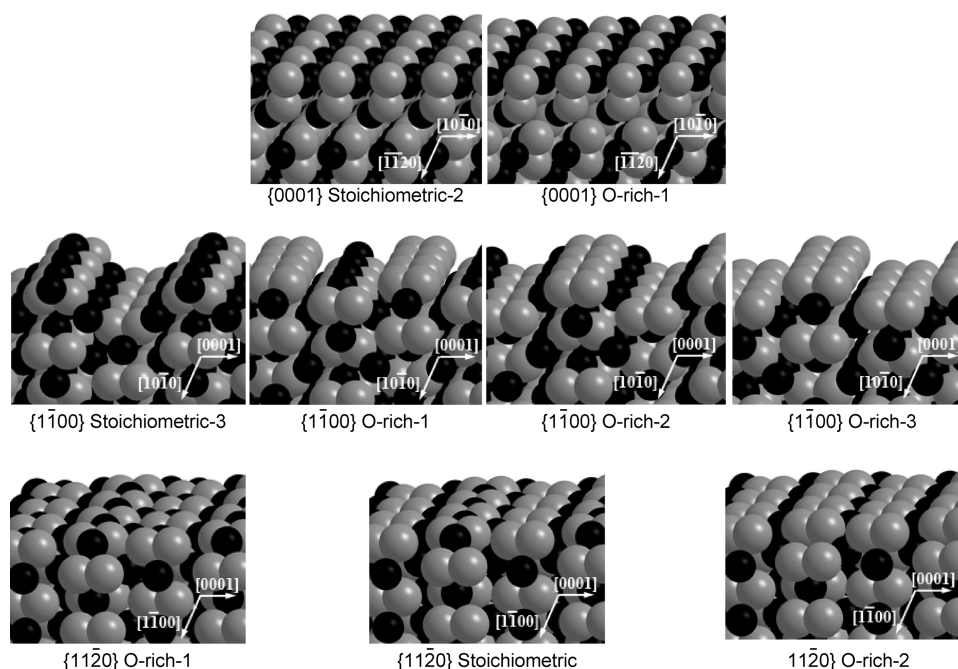
Figure 3. Structures of low-energy Li_2O_2 surfaces. Gray and black spheres represent O and Li atoms, respectively.
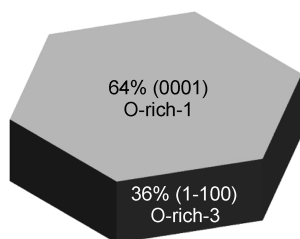
Figure 4. Equilibrium shape of Li_2O_2 crystallites based on calculated surface energies and the Wulff construction. The termination and relative areal fractions of basal and prismatic facets are identified.

energy surface overall and suggests that this surface will play an important role in surface reactions involving Li_2O_2.

The morphology of Li_2O_2 particles formed during discharge has been examined using SEM (scanning electronic microscopy), and they appear to exhibit a toroidal or "donutlike" shape reminiscent of red blood cells.[14] While the low aspect ratio of these deposits appears to be in rough agreement with our theoretical predictions, the curvature of the deposits suggests a somewhat higher degree of isotropy in the surface energy. We speculate that the latter may be due to the influence of the electrolyte, which is omitted in our treatment. In addition, since the energies for some of the surfaces differ on a per atom basis by less than k_BT (e.g., O-rich-3 $\{1\bar{1}00\}$ and O-

rich-2 $\{11\bar{2}0\}$, Table 2, right column), thermal effects may also lead to a more isotropic particle morphology.

4.2.2. Li_2O Surfaces. A noteworthy trend regarding the relative stabilities of Li_2O_2 surfaces is that oxygen-rich surfaces are generally more stable than lithium-rich or stoichiometric surfaces. This behavior differs from what is observed in Li_2O surfaces, where stoichiometric terminations are universally preferred, as we now describe. For Li_2O the surface free energies of 17 distinct terminations were examined from the low-index $\{100\}$, $\{110\}$, and $\{111\}$ facets, Figure 2 bottom panel. In all cases the most stable surfaces are stoichiometric, with a rank ordering of $\{111\}$ ($\gamma = 30$ meV/Å^2) < $\{110\}$ ($\gamma = 56$ meV/Å^2) < $\{100\}$ ($\gamma = 75$ meV/Å^2). Similar results were obtained in ref 24. On the basis of the Wulff construction, the equilibrium crystallite morphology is an octahedron with $\{111\}$ facets comprising 100% of the surface area. Our calculations predict that the termination of this facet (Figure 5, right) has Li^+ ions as the outermost surface layer, which is in agreement with the morphology suggested by experiments.[51] Indeed, $\{111\}$ surfaces are the natural cleavage plane for fluorite and antifluorite crystals; cleavage along these planes generates nonpolar surfaces by separating adjacent atomic planes having like charge.[53]

4.3. Surface Electronic Structure. In addition to examining the surface thermodynamics of Li_2O_2 and Li_2O, we have also performed a detailed study of the electronic structure
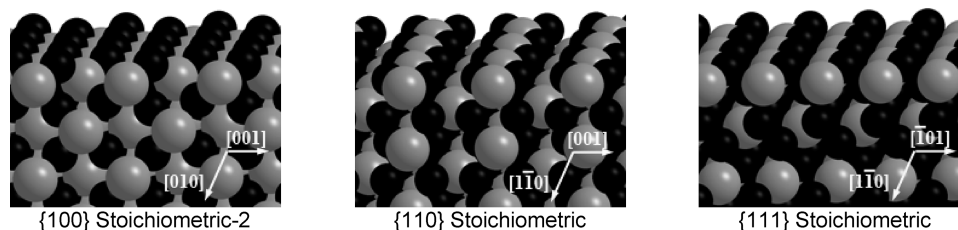
Figure 5. Structures of low-energy Li_2O surfaces. Gray and black spheres represent O and Li atoms, respectively.
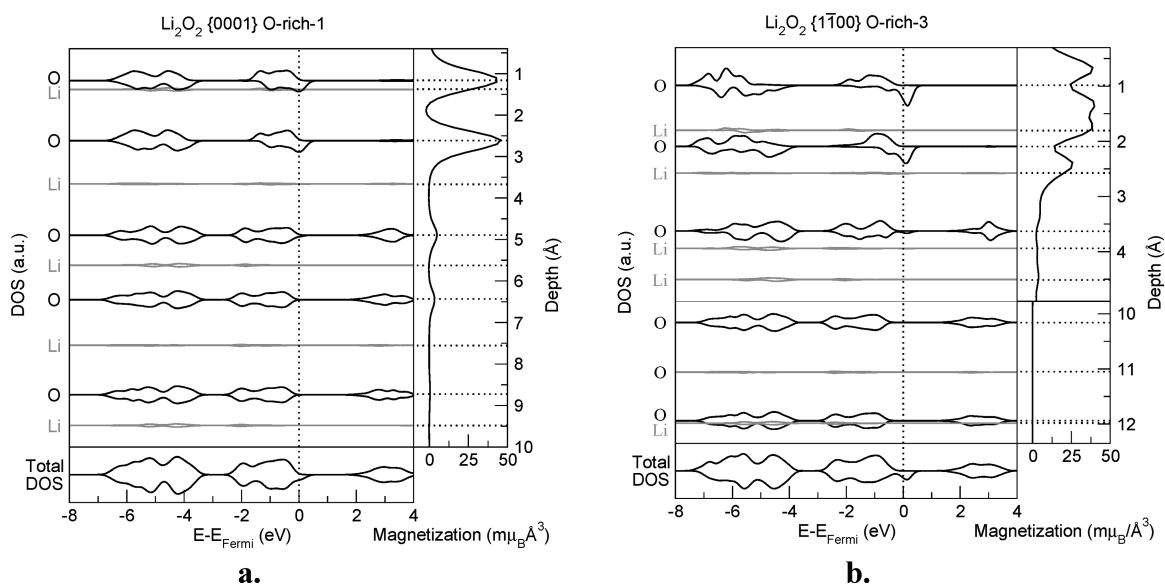
Figure 6. Calculated layer-projected spin density of states and planar-averaged magnetization for the energetically preferred surfaces of Li_2O_2: (a) {0001} O-rich-1, (b) {1$\bar{1}$00} O-rich-3. The positions of the DOS traces are staggered vertically to reflect the relative spacing of the atomic layers. Black traces are for oxygen layers, and gray traces are for lithium layers. In the magnetization density plots horizontal dotted lines indicate the positions of the atomic planes.

of the stable surface terminations. As mentioned above, Li_2O_2 and Li_2O differ significantly in their electrochemical reversibility despite having similar thermodynamic and bulk insulating properties. Given our observation of distinct surface stoichiometries between these compounds (i.e., Li_2O_2 surfaces are polar and O-rich, whereas Li_2O surfaces are stoichiometric and nonpolar) and known correlations linking surface termination with localized metallic behavior,[54] we hypothesized that differences in electrochemical behavior could be related to electronic structure at surfaces. Support for this assertion comes from prior studies showing that the oxygen-terminated surfaces of some metal oxides exhibit half-metallic behavior.[55] (Half-metallicity occurs in magnetic compounds or regions in which one spin channel is metallic and the other is insulating.) It is also known that Li_2O_2 deposits can be imaged using SEM without application of a conductive coating, which is typically needed for insulating compounds.[14] Below we examine the extent to which surface structure and composition impact surface electronic structure and discuss possible implications for battery performance.

Figure 6a shows the layer-projected spin density of states (DOS) for the most stable Li_2O_2 surface ({0001} O-rich-1) alongside its planar-averaged magnetization density. (In these calculations thicker slabs as well as finer k-point and fast Fourier transform (FFT) meshes were used to carefully characterize the spatial variation in electronic structure as a function of distance from the surface. For example, the Li_2O_2 {0001} O-rich-1 slab contained 43 layers and was 42.3 Å tall, including a 10 Å vacuum region.) In the figure the DOS for each layer is staggered vertically in proportion to the spacing of the atomic layers within the slab. From the total DOS (bottom panel), which averages the DOS from all layers in the slab, one can see that at least some portion of the slab exhibits ferromagnetic behavior. Moreover, the spin-up states are insulating, while the spin-down states are conducting, indicating that this geometry is indeed half-metallic. The layer-projected DOS further indicates that the conducting states and magnetism are localized on the two oxygen atoms comprising the O_2 anionic

dimer nearest the surface (top portion of figure); progressing deeper into the slab results in a return to a bulklike DOS with a band gap of ~2 eV and a nonmagnetic spin state.

The electronic structure of Li_2O_2 can be interpreted in terms of a tight-binding model. The valence band consists of oxygen 2p-derived π^* (antibonding) peroxide levels, while the upper and lower portions of the band below consist of bonding π and σ_p peroxide levels, respectively. The spatial distribution of the magnetization density (Figure 6a, right) suggests that magnetic behavior arises from electrons in the π^* peroxide orbitals. That is, each O atom in the surface dimer is surrounded by a torus of magnetization that lies in a plane orthogonal to the dimer axis, and a nodal plane separates the two O atoms. [As shown in Figure 3 (top left), the O_2 dimers in this surface are aligned parallel to the surface normal.] The total magnetization of this surface is found to be 57 $m\mu_B/Å^2$. (We note that surface magnetism has also been reported in DFT calculations on small clusters of Li_2O_2.[56]) Figure 7 shows the surface projection of the band structure, which identifies the metallic behavior as arising from two partially depleted valence-band-derived spin-down surface states that cross the Fermi level (each of these states has a degeneracy of 2 because the supercell contains two surfaces). The emergence of these surface states is consistent with the charge compensation behavior typical of stable polar surfaces.[52−54] An analysis of the charge density for the surface band at the Γ-point (Figure S2, Supporting Information) confirms the extensive properties of this wave function. Additional tests using the HSE06 hybrid functional (Figure S3, Supporting Information) have verified the half-metallic behavior predicted by the PBE GGA.

The {1$\bar{1}$00} O-rich-3 surface—which comprises the rim of the predicted Li_2O_2 crystallite morphology (Figure 4)—was also found to be half-metallic, as shown in Figure 6b, with a surface magnetization of 82 $m\mu_B/Å^2$. The slab for this surface contained 42 layers, and the supercell was 32.8 Å tall. The spatial variation in the magnetization density again suggests that magnetism arises from the π^* oxygen orbitals localized at the surface. Note that in this case the magnetization density shows
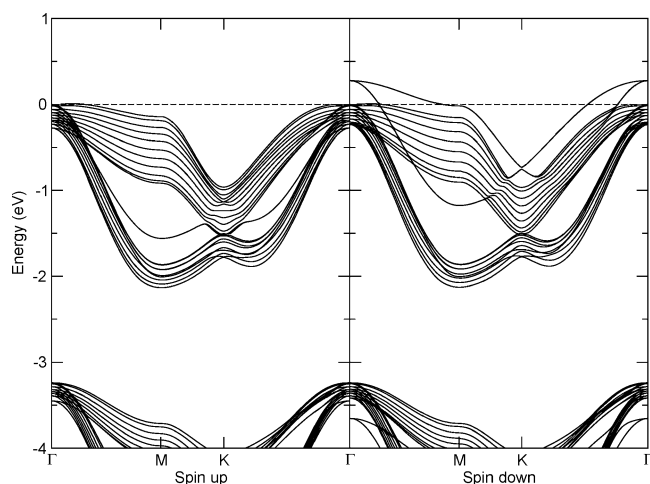
Figure 7. Surface band structure for the most stable Li_2O_2 {0001} surface, O-rich-1. The horizontal dashed line represents the Fermi level. Spin-up and spin-down bands are shown in the left and right panels, respectively.

shallow minima at the O sites, unlike in the {0001} surface, because the O_2 dimers are now oriented parallel to the surface.

Figure 8 shows the layer-projected density of states for the most stable Li_2O surface ({111} stoichi) from an 18-layer 24.6
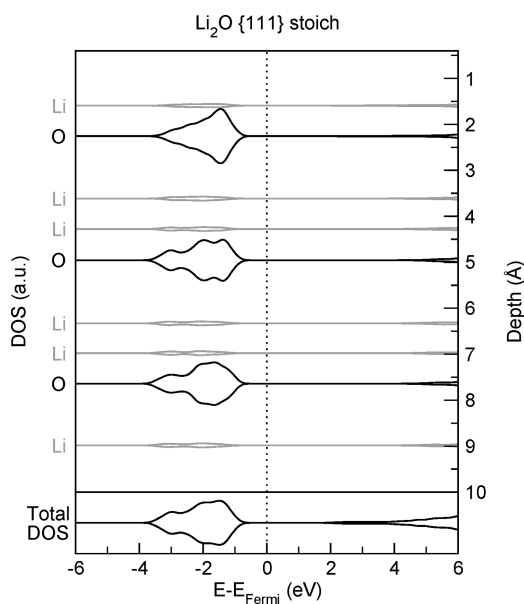
Figure 8. Calculated layer-projected spin density of states for the most stable surface of Li_2O, {111} stoichi.

Å slab. In contrast to the behavior of the Li_2O_2 surfaces, this surface exhibits insulating and nonmagnetic behavior throughout the entire thickness of the slab. Similar insulating behavior was observed in the other stable (stoichiometric) {100} and {110} surfaces. The absence of half-metallic behavior in Li_2O can be traced to the fact that its stable surfaces are stoichiometric; as described above, half-metallic behavior typically appears only in oxygen-rich surfaces.

Since electrochemical phenomena are generally confined to surfaces and interfaces, the presence (or absence) of an electrically conductive surface region should strongly impact reactions that occur on or near those surfaces. Thus, we

speculate that the insulating nature of Li_2O surfaces may contribute to the poor electrochemical reversibility of this phase in comparison to Li_2O_2. Indeed, with the exception of nanoscale displacement reactions (which do not require Li_2O to participate in charge transfer), Li_2O is generally thought to be electrochemically inactive.[57,58] For example, recent experiments using Li−oxygen cells preloaded with lithium oxides have shown that while Li_2O_2 can readily be decomposed, Li_2O cannot be oxidized even when charged to 4.6 V.[21]

In prior studies the half-metallicity of O-rich surfaces in other metal oxides[55] has been attributed to a loss of coordination of (and charge transfer to) the surface O atoms, resulting in the formation of 2p holes in the valence band.[55] [A similar effect occurs in bulk Li_2O_2: Hummelshøj et al. have shown that a high concentration of lithium vacancies produce conductivity in bulk Li_2O_2 by creating holes in the valence band.[23]] We have confirmed that this mechanism is also at play in Li_2O_2 by performing a Bader charge-partition analysis,[59] the results of which are shown in Table 3. [There is a small fluctuation in the Bader charge of O atoms in the Li_2O_2 {0001} slab due to the coarseness of the charge density grid. In the slab centers and bulk Li_2O_2, the Bader charge was averaged over symmetry-equivalent O sites.] The Bader analysis indicates that there is significant charge depletion at the surface O sites for the two most stable Li_2O_2 surfaces, consistent with valence band hole formation and with what has been reported for other half-metallic oxides.[55] For both the {0001} and {1$\bar{1}$00} surfaces, the two oxygen layers nearest the surface account for nearly all of the electron depletion and magnetization, while the surface lithium sites, which are nominally highly ionized, experience no change in their charge state or magnetization. In the case of the basal surface, the top two oxygen layers have, respectively, 6.58 and 6.73 electrons associated with their Bader volumes. In comparison, oxygen in bulk Li_2O_2 attracts 6.85 electrons. The surface electron deficiency is even larger in the prismatic surface ($Q = 6.40$ and 6.50), resulting in relatively larger induced magnetic moments. In contrast, in the Li_2O surface (Table 3, right) there is essentially no difference in charge partitioning, and therefore no magnetism, across the thickness of the slab. Overall, the magnitudes of the calculated magnetic moments on the Li_2O_2 surface O sites (0.22−0.52 μ_B) are somewhat less than that found in bulk nickel, 0.62 μ_B.[50] The total magnetization in each slab corresponds very nearly to one unpaired electron for each lithium atom removed from a stoichiometric surface: in a {0001} O-rich-1 unit cell, the surface is deficient half a Li atom, and in the {1$\bar{1}$00} O-rich-3 unit cell the surface is deficient two Li atoms. In the case of the {1$\bar{1}$00} O-rich-3 surface there are two atomic sites per O layer. Thus, the magnetization reported in Table 3, which is averaged over both oxygens, should be doubled to obtain the absolute value of the magnetization.

We find that half-metallicity in oxygen-rich stoichiometries is quite robust across Li−O phases: all of the oxygen-rich slabs we have explored in Li_2O_2 and Li_2O exhibit this behavior regardless of their stability. A survey of the metallic/insulating trends across the Li-rich and stoichiometric slabs reveals behavior consistent with the filling of surface states in ionic compounds.[52,53] For example, we find that the low-energy stoichiometric surfaces in Li_2O are insulating and that Li-rich polar surfaces can exhibit nonmagnetic metallic behavior through partial filling of conduction band-derived surface states.

As the {0001} O-rich-1 surface exhibits the lowest formation energy and should comprise a majority of the crystallite surface

Table 3. Bader Charge and Magnetization Partitioning of the Most Stable Li_2O_2 and Li_2O Surfaces as a Function of Depth within the Surface Slab[a]

layer no.	Li_2O_2 {0001} O-rich-1			Li_2O_2 {1$\bar{1}$00} O-rich-3			Li_2O {111} stoichi		
	atom	Q	μ	atom	Q	μ	atom	Q	μ
1	O	6.58	0.22	O	6.40	0.52	Li	0.16	0.00
2	Li	0.16	0.00	Li	0.17	0.00	O	7.66	0.00
3	O	6.73	0.23	O	6.50	0.40	Li	0.18	0.00
4	Li	0.14	0.00	Li	0.14	0.00	Li	0.18	0.00
5	O	6.84	0.02	O	6.82	0.05	O	7.64	0.00
6	Li	0.16	0.00	Li	0.17	0.00	Li	0.18	0.00
7	O	6.83	0.01	Li	0.16	0.00	Li	0.18	0.00
8	Li	0.14	0.00	O	6.82	0.04	O	7.64	0.00
9	O	6.87	0.00	Li	0.14	0.00	Li	0.18	0.00
10	Li	0.16	0.00	O	6.85	0.00			
slab center	Li	0.14/0.16	0.00	Li	0.14/0.16	0.00	Li	0.18	0.00
	O	6.85	0.00	O	6.85	0.00	O	7.64	0.00
bulk	Li	0.14/0.16	0.00	Li	0.14/0.16	0.00	Li	0.18	0.00
	O	6.85	0.00	O	6.85	0.00	O	7.64	0.00

[a]Layer 1 corresponds to the surface. Q refers to the number of electrons associated with atoms within a given atomic layer, and μ is the magnetization in Bohr magnetons. "Bulk" and "slab center" refer to the values obtained from a separate bulk calculation and from the center region of the surface slabs, respectively. The two values shown for Li in Li_2O_2 correspond to the two symmetry-inequivalent sites. In the Li_2O_2 {1$\bar{1}$00} slab, where two O atoms lie in each O layer, the Bader charge has been averaged over these two sites.

area, we speculate that it could play a significant role in the electron transport properties of Li_2O_2. To assess the magnitude of this effect, we have estimated the conductivity of this surface using the calculated density of states (Figure 6a) and surface band structure (Figure 7). Assuming the surface states can be approximated as isotropic, the following expression for the 2D conductivity can be derived from the Boltzmann transport equation:[60]

$$\sigma_s = \frac{e^2}{2}(\tau v_f)v_f D^{2D} \tag{6}$$

Here τ is the carrier relaxation time, $v_f = (1/\hbar)(\partial E/\partial k)$ is the Fermi velocity, and D^{2D} is the 2D density of states. We approximate the {0001} surface states as isotropic by taking an average of the Fermi velocity at two points on the Fermi ring: one on the line connecting Γ and K, and one on the line connecting Γ and M. Averaging also over the two surface bands yields $v_f = 2.07 \times 10^7$ cm/s. From the calculated DOS we find that $D^{2D} \approx 3$ states/(unit cell·eV). Lacking knowledge of the dominant scattering mechanism, it is necessary to estimate the carrier relaxation time τ, as an explicit calculation is beyond the scope of this study. On the basis of a survey of values reported for other materials, we take $\tau = 1$ fs, which we believe represents a reasonable lower bound. For example, the carrier relaxation time in metals is typically an order of magnitude larger,[61] and values for other compounds include 1–10 fs[62] in transparent conducting oxides, 200 fs[63] in ultrathin layers of n-doped GaAs, and 400 and 100 fs[64] in bulk and nanostructured TiO_2. Adopting this value for τ, the surface conductivity of the {0001} surface is calculated to be $\sigma_s \approx 10^{-4}$ Ω^{-1}/□. This value is comparable to those of other conducting surfaces, such as Ag superstructures on a Si {111} surface ($\sigma_s \approx 10^{-4}$ Ω^{-1}/□)[60] or hydrogenated diamond films ($\sigma_s \approx 10^{-4}$–10^{-5} Ω^{-1}/□),[65] but much larger than those of insulating surfaces, such as undoped diamond ($\sigma_s \approx 10^{-8}$ Ω^{-1}/□ or less).[65] One can also interpret the surface conductivity as a bulk conductivity associated with a thin conducting "skin" at the surface of Li_2O_2 particles. Taking the skin thickness as equal to the depth that metallic behavior

penetrates into the bulk (~4 Å), this region has an effective bulk conductivity of 10^5 Ω^{-1}/m. This value is comparable to the bulk conductivity of stainless steel (10^6 Ω^{-1}/m)[50] and larger than the bulk conductivities associated with the Nafion-bonded carbon cathodes used in Li−air cells (~10^2 Ω^{-1}/m).[14] To the best of our knowledge, an experimental measurement of the surface conductivity of Li_2O_2 has not been reported. Measurements of this type would be an important addition to our understanding of the surface properties of Li−O phases and are left as a challenge to the experimental community.

Given our estimate for conductivity along Li_2O_2 surfaces, we conclude by examining the extent to which surface transport of electrons may contribute to the overpotentials observed during cell operation. To do so, we treat the agglomeration of Li_2O_2 particles formed during discharge as resistors in parallel, and we approximate each particle as a square (note that the surface resistance of a square is independent of its size). To emphasize the role of transport within particles, we neglect contact resistances, which of course could be significant in real systems. For discharge at 100 mA/g_{carbon}, the diameter of Li_2O_2 particles is observed to be approximately 350 nm and the capacity to be 3000 (mA h)/g_{carbon}.[14] On the basis of these values, the number of Li_2O_2 particles is approximately 10^{14} per gram of carbon. Since each particle contributes a conductivity of approximately 10^{-4} Ω^{-1}, the total conductance associated with the surfaces is on the order of 10^{10} Ω^{-1}/g_{carbon}. At a discharge rate of 100 mA/ g_{carbon}, this resistance will produce a voltage drop on the order of 10^{-11} V, which is negligible compared to the experimentally observed overpotentials in Li−air cells. (The actual voltage drop is likely some orders of magnitude larger, as the particles/ resistors will not be in parallel if the discharge product forms a thick layer.) Due to the presence of conducting surfaces, we therefore conclude that (given sufficient accessible surface area), electron transport through Li_2O_2 particles will not be a significant limiting factor in the performance of Li−air batteries. Similarly, we anticipate that grain boundaries could also serve as electrically conductive pathways in Li_2O_2 if they exhibit oxygen-rich stoichiometries. We note that Albertus et al. have argued

that electrical passivation (arising from the growth of an insulating Li−O discharge phase) may limit capacity in Li−oxygen cells.[31] Our results suggest otherwise. That is, discharge morphologies exhibiting a high density of planar defects (e.g., surfaces and grain boundaries) may provide pathways for electron conduction that would offset passivation effects.

5. CONCLUSION

Achieving viable secondary Li−oxygen batteries will hinge upon the identification and understanding of mechanisms that most strongly control their performance. Since the operation of these batteries involves the formation, growth, and subsequent decomposition of Li−O particles, we anticipate that surface phenomena associated with these compounds may contribute to the overpotentials and rate limitations observed in these systems. Toward a more thorough understanding of these issues, we have used DFT calculations to characterize the thermodynamics and electronic structures of 40 distinct surfaces of Li_2O_2 and Li_2O. Our calculations have identified several Li_2O_2 surface terminations that are more stable than those previously reported in the literature, and application of the Wulff construction reveals that an oxygen-rich basal surface (O-rich-1) constitutes the majority of the Li_2O_2 crystallite surface area. While the most stable Li_2O_2 surfaces are oxygen rich, the low-energy surfaces of Li_2O are stoichiometric, with the {111} facet being the most stable overall. These differences in stoichiometry translate to dramatic differences in surface electronic structure, despite the fact that Li_2O_2 and Li_2O are both bulk insulators. More specifically, the reduced coordination of oxygen atoms at Li_2O_2 surfaces results in the formation of a thin metallic and ferromagnetic region (i.e., half-metallic behavior) localized at the surface, with an estimated electrical conductivity of ∼10^5 Ω^{-1}/m. In contrast, Li_2O surfaces are predicted to be insulating and nonmagnetic, consistent with extant models of surface electronic structure in ionic compounds. The existence of facile pathways for electron transport along Li_2O_2 surfaces—and the absence of the same in Li_2O—may explain observations of electrochemical reversibility in systems where Li_2O_2 is the discharge product and the irreversibility of systems that discharge to Li_2O. It also suggests that electron transport through well-connected Li_2O_2 particles may not significantly hinder performance (e.g., reduce capacity) in Li−oxygen cells.

■ ASSOCIATED CONTENT

Ⓢ Supporting Information

Sensitivity of the results with respect to O_2 overbinding correction, electronic structure of half-metallic surface states, and ball and stick figures for all surface structures examined in this study. This material is available free of charge via the Internet at http://pubs.acs.org.

■ AUTHOR INFORMATION

Corresponding Author
djsiege@umich.edu

■ ACKNOWLEDGMENTS

■ REFERENCES

(1) Cairns, E. J.; Albertus, P. *Annu. Rev. Chem. Biomol. Eng.* **2010**, *1*, 299.
(2) *Energy Storage System Goals*, U.S. Advanced Battery Consortium: Southfield, MI, 2006.
(3) Beattie, S. D.; Manolescu, D. M.; Blair, S. L. *J. Electrochem. Soc.* **2009**, *156*, A44.
(4) Girishkumar, G.; McCloskey, B.; Luntz, A. C.; Swanson, S.; Wilcke, W. *J. Phys. Chem. Lett.* **2010**, *1*, 2193.
(5) Lu, Y. C.; Gasteiger, H. A.; Parent, M. C.; Chiloyan, V.; Shao-Horn, Y. *Electrochem. Solid State Lett.* **2010**, *13*, A69.
(6) McCloskey, B. D.; Bethune, D. S.; Shelby, R. M.; Girishkumar, G.; Luntz, A. C. *J. Phys. Chem. Lett.* **2011**, *2*, 1161.
(7) Freunberger, S. A.; Chen, Y. H.; Peng, Z. Q.; Griffin, J. M.; Hardwick, L. J.; Barde, F.; Novak, P.; Bruce, P. G. *J. Am. Chem. Soc.* **2011**, *133*, 8040.
(8) Xiao, J.; Hu, J. Z.; Wang, D. Y.; Hu, D. H.; Xu, W.; Graff, G. L.; Nie, Z. M.; Liu, J.; Zhang, J. G. *J. Power Sources* **2011**, *196*, 5674.
(9) Xu, W.; Viswanathan, V. V.; Wang, D. Y.; Towne, S. A.; Xiao, J.; Nie, Z. M.; Hu, D. H.; Zhang, J. G. *J. Power Sources* **2011**, *196*, 3894.
(10) Mizuno, F.; Nakanishi, S.; Kotani, Y.; Yokoishi, S.; Iba, H. *Electrochemistry* **2010**, *78*, 403.
(11) Chase, M. W. *NIST-JANAF Thermochemical Tables*, 4th ed.; American Institute of Physics: Melville, NY, 1998.
(12) Abraham, K. M.; Jiang, Z. *J. Electrochem. Soc.* **1996**, *143*, 1.
(13) Debart, A.; Bao, J.; Armstrong, G.; Bruce, P. G. *J. Power Sources* **2007**, *174*, 1177.
(14) Lu, Y. C.; Kwabi, D. G.; Yao, K. P. C; Harding, J. R.; Zhou, J. G.; Zuin, L.; Shao-Horn, Y. *Energy Environ. Sci.* **2011**, *4*, 2999.
(15) Laoire, C. O.; Mukerjee, S.; Plichta, E. J.; Hendrickson, M. A.; Abraham, K. M. *J. Electrochem. Soc.* **2011**, *158*, A302.
(16) Ogasawara, T.; Debart, A.; Holzapfel, M.; Novak, P.; Bruce, P. G. *J. Am. Chem. Soc.* **2006**, *128*, 1390.
(17) Read, J. *J. Electrochem. Soc.* **2002**, *149*, A1190.
(18) Thapa, A. K.; Saimen, K.; Ishihara, T. *Electrochem. Solid State Lett.* **2010**, *13*, A165.
(19) Zhang, S. S.; Foster, D.; Read, J. *J. Power Sources* **2010**, *195*, 1235.
(20) Thapa, A. K.; Ishihara, T. *J. Power Sources* **2011**, *196*, 7016.
(21) Xu, W.; Xu, K.; Viswanathan, V. V.; Towne, S. A.; Hardy, J. S.; Xiao, J.; Nie, Z.; Hu, D.; Wang, D.; Zhang, J.-G. *J. Power Sources* **2011**, *196*, 9631.
(22) Xu, Y.; Shelton, W. A. *J. Chem. Phys.* **2010**, *133*, 024703.
(23) Hummelshoj, J. S.; Blomqvist, J.; Datta, S.; Vegge, T.; Rossmeisl, J.; Thygesen, K. S.; Luntz, A. C.; Jacobsen, K. W.; Norskov, J. K. *J. Chem. Phys.* **2010**, *132*, 071101.
(24) Seriani, N. *Nanotechnology* **2009**, *20*, 445703.
(25) Kumar, B.; Kumar, J.; Leese, R.; Fellner, J. P.; Rodrigues, S. J.; Abraham, K. M. *J. Electrochem. Soc.* **2010**, *157*, A50.
(26) Lu, Y. C.; Xu, Z. C.; Gasteiger, H. A.; Chen, S.; Hamad-Schifferli, K.; Shao-Horn, Y. *J. Am. Chem. Soc.* **2010**, *132*, 12170.
(27) Debart, A.; Paterson, A. J.; Bao, J.; Bruce, P. G. *Angew. Chem., Int. Ed.* **2008**, *47*, 4521.
(28) Lu, Y. C.; Gasteiger, H. A.; Shao-Horn, Y. *Electrochem. Solid State Lett.* **2011**, *14*, A70.
(29) Lu, Y. C.; Gasteiger, H. A.; Crumlin, E.; McGuire, R.; Shao-Horn, Y. *J. Electrochem. Soc.* **2010**, *157*, A1016.
(30) Wulff, G. *Z Krystallogr. Mineral.* **1901**, *34*, 449.
(31) Albertus, P.; Girishkumar, G.; McCloskey, B.; Sanchez-Carrera, R. S.; Kozinsky, B.; Christensen, J.; Luntz, A. C. *J. Electrochem. Soc.* **2011**, *158*, A343.
(32) Ishii, Y.; Murakami, J.; Itoh, M. *J. Phys. Soc. Jpn.* **1999**, *68*, 696.
(33) Chen, J. Z.; Hummelshoj, J. S.; Thygesen, K. S.; Myrdal, J. S. G.; Norskov, J. K.; Vegge, T. *Catal. Today* **2011**, *165*, 2.
(34) Ferapontov, Y. A.; Kokoreva, N. V.; Kozlova, N. P.; Ul'yanova, M. A. *Russ. J. Gen. Chem.* **2009**, *79*, 891.

(35) Perdew, J. P.; Burke, K.; Ernzerhof, M. *Phys. Rev. Lett.* **1996**, *77*, 3865.

(36) Kresse, G.; Furthmuller, J. *Comput. Mater. Sci.* **1996**, *6*, 15.

(37) Kresse, G.; Furthmuller, J. *Phys. Rev. B* **1996**, *54*, 11169.

(38) Kresse, G.; Hafner, J. *Phys. Rev. B* **1993**, *47*, 558.

(39) Kresse, G.; Hafner, J. *Phys. Rev. B* **1994**, *49*, 14251.

(40) Blochl, P. E. *Phys. Rev. B* **1994**, *50*, 17953.

(41) Kresse, G.; Joubert, D. *Phys. Rev. B* **1999**, *59*, 1758.

(42) Monkhorst, H. J.; Pack, J. D. *Phys. Rev. B* **1976**, *13*, 5188.

(43) Wallace, D. C. *Thermodynamics of Crystals*; John Wiley & Sons: New York, 1972.

(44) Wei, S. Q.; Chou, M. Y. *Phys. Rev. Lett.* **1992**, *69*, 2799.

(45) Kurth, S.; Perdew, J. P.; Blaha, P. *Int. J. Quantum Chem.* **1999**, *75*, 889.

(46) Wang, L.; Maxisch, T.; Ceder, G. *Phys. Rev. B* **2006**, *73*, 6.

(47) Reuter, K.; Scheffler, M. *Phys. Rev. B* **2002**, *65*.

(48) Foppl, H. *Z. Anorg. Allg. Chem.* **1957**, *291*, 12.

(49) Cota, L. G.; de la Mora, P. *Acta Crystallogr., Sect. B: Struct. Sci.* **2005**, *61*, 133.

(50) *CRC Handbook of Chemistry and Physics*, 91st ed.; CRC Press/Taylor and Francis: Boca Raton, FL, 2011.

(51) Taylor, D. *Trans. J. Br. Ceram. Soc.* **1984**, *83*, 32.

(52) Berliner, R.; Fajen, O.; Smith, H. G.; Hitterman, R. L. *Phys. Rev. B* **1989**, *40*, 12086.

(53) Tasker, P. W. *J. Phys. C: Solid State Phys.* **1979**, *12*, 4977.

(54) Claudine, N. *J. Phys.: Condens. Matter* **2000**, *12*, R367.

(55) Gallego, S. B., J. I.; Cerda, J.; Munoz, M. C. *J. Phys.: Condens. Matter* **2005**, *17*, L451.

(56) Lau, K. C. C., L.A.; Greeley, J. Presented at the 4th Symposium on Energy Storage: Beyond the Lithium Ion, Richland, WA, 2011.

(57) Obrovac, M. N. D., R. A.; Sanderson, R. J.; Dahn, J. R. *J. Electrochem. Soc.* **2001**, *148*, A576.

(58) Poizot, P. L., S.; Grugeon, S.; Dupont, L.; Tarascon, J.-M. *Nature* **2000**, *407*, 496.

(59) Bader, R. F. W. *Atoms in Molecules—A Quantum Theory*; Oxford University Press: Oxford, U.K., 1990.

(60) Matsuda, I. H., T.; Konishi, M.; Liu, C.; Morikawa, H.; D'angelo, M.; Hasegawa, S.; Okuda, T.; Kinoshita, T. *Phys. Rev. B* **2005**, *71*, 235315.

(61) *McGraw-Hill Encyclopedia of Science & Technology*, 10th ed.; McGraw-Hill: New York, 2007.

(62) Kaydanov, V. I. C., T. J.; Young, D. L. Presented at the Materials Research Society Workshop, Denver, CO, 2000.

(63) Funk, S. A., G.; Handloser, M.; Kersting, R *Opt. Express* **2009**, *17*, 17450.

(64) Hendry, E.; Koeberg, M.; O'Regan, B.; Bonn, M. *Nano Lett.* **2006**, *6*, 755.

(65) Andriotis, A. N. M., G.; Richter, E.; Menon, M. *Phys. Rev. Lett.* **2008**, *100*, 106801.